

Supplementary Material - A novel pyrochlore-like crystal with a photonic band gap self-assembled using colloids with a simple interaction potential

Harini Pattabhiraman,* Guido Avvisati, and Marjolein Dijkstra[†]
*Soft Condensed Matter, Debye Institute for Nanomaterials Science, Department of Physics,
 Utrecht University, Princetonplein 5, 3584 CC Utrecht, The Netherlands*

(Dated: August 21, 2017)

STRUCTURE OF COLUMNAR PHASE

The hexagonal columnar phase in our system is spontaneously formed either by (1) compressing an isotropic fluid phase to higher densities at constant temperature in the NPT ensemble, or (2) cooling a crystal phase to lower temperature in the NVT ensemble. An overview of the configurations of this phase as obtained in our simulations is given in Fig. 1. Fig. 1a and 1b display the configuration in different orientations. We note the ordering of particles into columns, which are positioned on a hexagonal lattice. In Fig. 1c, we present the planar view of particles, which are arranged to strings. We note the ordering of particles in the planes perpendicular to the column axis, while the position of particles along the column axis is irregular. This column axis can be seen as the individual strings in Fig. 1c. The incentive for the particles to form these strings is to reduce the number of nearest neighbours, which results in a reduction of the potential energy of the system. The strings are arranged in such a way that each particle has only two neighbours along the string, and the distance between the neighbour-

ing strings is larger than the shoulder width thereby resulting in no overlapping coronas between them. Similar columnar structures have also been reported for experimental systems of gold nanoparticles functionalized with promesogenic (liquid crystal forming) ligands [1, 2]. We want to point out that this phase, when spontaneously formed as in the current case, can serve as a template for the fabrication of porous materials, both in its direct or inverse form, as shown in Fig. 1b and 1d. Such a self assembly of inexpensive porous nanomaterials can be an alternative to molecular caged structures such as zeolites and can be used in applications involving filtration, size-selection, or catalysis [3].

STABILITY RANGE OF THE PYROCHLORE-LIKE STRUCTURE

In order to assess the robustness of the pyrochlore-like phase (PYR), we performed simulations in the NVT ensemble over a range of densities, temperatures, shoulder widths and system sizes. We first present a comparison between the ideal pyrochlore (iPYR) and PYR obtained

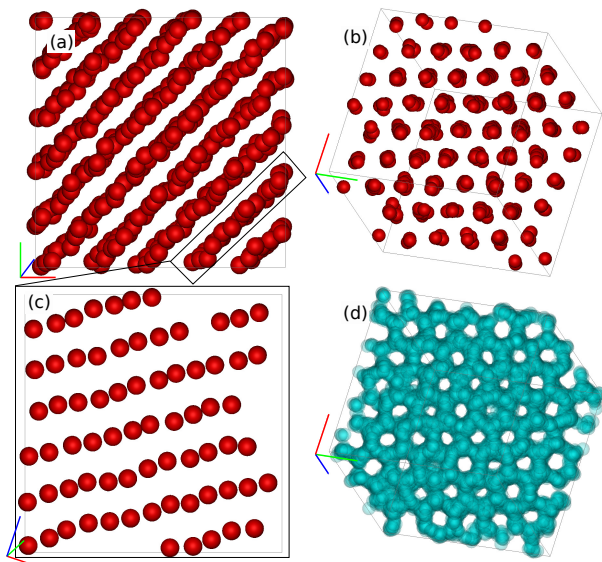


FIG. 1. Hexagonal columnar phase (COL): (a,b) different orientations of the sample configuration of the COL phase as obtained in our simulations (c) cut-view showing the plane of strings (d) porous structure obtained by the distribution of voids (in blue) in the COL phase.

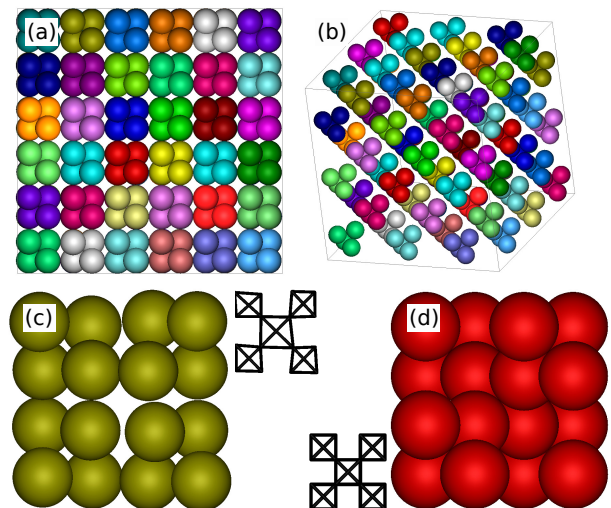


FIG. 2. Pyrochlore structure: (a,b) different orientations of the sample configuration of the pyrochlore (PYR) lattice obtained in our simulations. Only the hard-cores of the particles are drawn here and the colors represent different clusters. Unit cells of (c) PYR and (d) iPYR along with their bond structures.

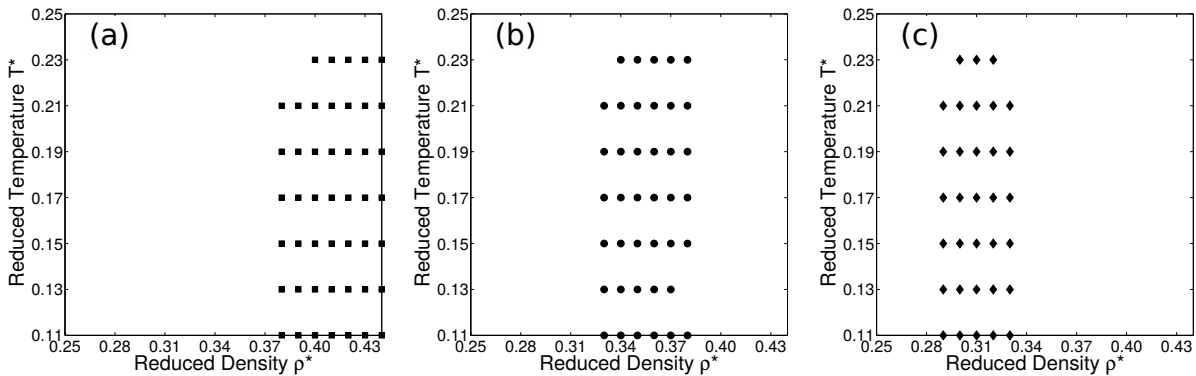


FIG. 3. State diagram in the temperature-density representation obtained for the HCSS system with shoulder width $\delta =$ (a) $1.95\sigma_{HS}$ (b) 2.10σ and (c) $2.25\sigma_{HS}$. The reduced quantities are defined as $T^* = k_B T/\epsilon$ and $\rho^* = N\sigma_{HS}^3/V$. The markers denote the region where the PYR phase is formed and the box denotes the parameter regime for which the simulations were carried out.

in our simulations and then present the effect of density, temperature, shoulder width and system size.

We present a comparison between the PYR and iPVR structures in Fig. 2. In Fig. 2a and Fig. 2b, we show different orientations of a sample configuration of our PYR, where the various clusters are marked by different colors. This clearly shows a layered arrangement of tetrahedral clusters. In Fig. 2c and Fig. 2d, we respectively show the unit cells of the PYR and iPVR structures. The insets show the bond structure between the neighboring particles. We note here that the central tetrahedron (seen as a square in this representation of bonds) of PYR is larger than the surrounding four tetrahedra which contrasts the equi-sized tetrahedra of the iPVR.

Shoulder width

To assess the range of formation of the PYR as a function of shoulder width, we performed a series of simulations in the NVT ensemble starting with the PYR structure. We varied the temperature $0.11 \leq T^* \leq 0.25$, density $0.25 \leq \rho^* \leq 0.44$ and shoulder width $1.95\sigma_{HS} \leq \delta \leq 2.25\sigma_{HS}$. We plot the state diagram in the temperature-density plane showing the mechanical stability region of the PYR in Fig. 3. Here, the state diagrams are plotted at the extreme shoulder widths $\delta = 1.95\sigma_{HS}$ and $2.25\sigma_{HS}$ and the intermediate shoulder width where the rest of the study was based $\delta = 2.10\sigma_{HS}$. The box represents the region of exploration. Firstly, we note that the PYR phase stays stable over a range of temperatures and densities at all three shoulder widths. Secondly, the region plotted in the state diagram at $\delta = 2.10\sigma_{HS}$ agrees well with the phase diagram given in Fig. 1 of the manuscript. Lastly, we find that the range of density where the PYR forms increases with decreasing shoulder width. This is to be expected as with decreasing shoulder width, the tetrahe-

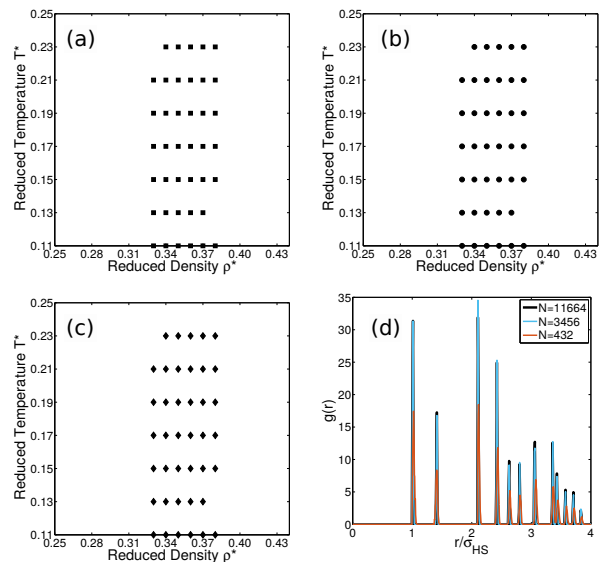


FIG. 4. State diagram in the temperature-density representation obtained for the HCSS system with shoulder width $\delta = 2.10\sigma$ using system sizes of (a) 432 (b) 3456 and (c) 11664 particles. The markers denote the region where the PYR phase is formed and the box denotes the parameter regime for which the simulations were carried out. (d) Pair correlation functions of the PYR phase calculated at different system sizes at $T^* = 0.15$ and $\rho^* = 0.37$. The reduced quantities are defined as $T^* = k_B T/\epsilon$ and $\rho^* = N\sigma_{HS}^3/V$.

dra can pack more closely without overlap of the coronas of the inter- and intra-tetrahedral neighbors.

System size

To assess the effect of the finite size of the system on the PYR formation, we performed a series of NVT simula-

tions starting with the PYR structure consisting of $N = 432, 3456, \text{ and } 11664$ particles. We varied the temperature $0.11 \leq T^* \leq 0.25$ and the density $0.25 \leq \rho^* \leq 0.44$ at a constant shoulder width $\delta = 2.10\sigma_{HS}$. The state diagrams are given in Fig. 4a-c. We find that the system size does not affect the mechanical stability region of the PYR phase. In addition, we present the pair correlation function $g(r)$ for varying system sizes calculated at density $\rho^* = 0.37$ and temperature $T^* = 0.15$ in Fig. 4d, showing that the structure of the PYR phase is hardly affected by the system size.

PHOTONIC BAND STRUCTURE CALCULATION

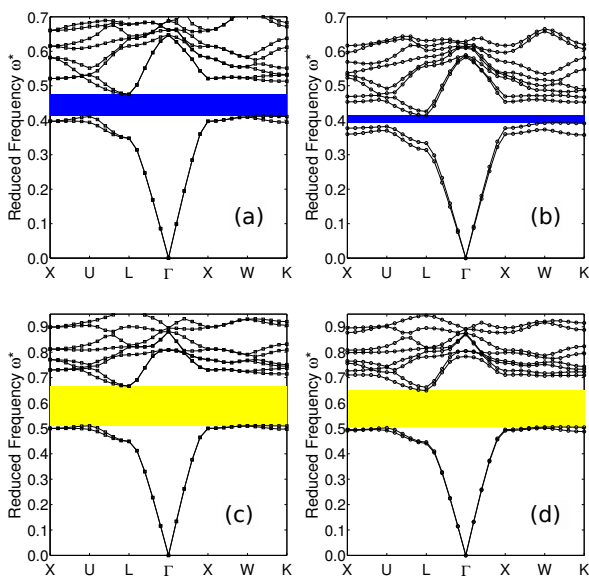


FIG. 5. Comparison of photonic band structures of pyrochlore structures namely, (a,c) the ideal pyrochlore lattice (iPYR) and (b,d) the pyrochlore-like structure (PYR) obtained in our simulations. Photonic band structures are calculated for (a,b) direct structure of silicon spheres in air and (c,d) inverse structure of air spheres in silicon at (reduced) density $\rho^* = N\sigma_{HS}^3/V =$ (a) 0.87 (b) 1.18 (c) 2.52 (d) 2.52. The reduced frequency is written as $\omega^* = \omega a/2\pi c$.

In Fig. 5, we present the photonic band structures calculated for the ideal pyrochlore lattice (iPYR) and the pyrochlore-like structure (PYR) obtained in our simulations. These band structures are calculated at the densities of maximum gap width for each of the structures. The band structure corresponding to iPYR is given in Figs. 5a and 5c and those of PYR in Figs. 5b and 5d. Figs. 5a and 5b denote the direct dielectric structures of silicon spheres in air and Figs. 5c and 5d denote the inverse structure of air spheres in silicon. In all these plots, we find that the upper bound of the band gap is decided by the L symmetry point and the lower bound

by the X symmetry point, as can be expected in the FCC (face-centered cubic) class of structures. Additionally, we find that all the bands above the band gap for the PYR structure given in Fig. 5b have moved downwards in frequency. Given that all parameters used in these two structures, namely PYR and iPYR, are the same, one could attribute this shifting of the bands to the observed peak splitting in PYR. It is worth noting that the band gap at the L symmetry point can likely be increased by using core-shell particles with a high dielectric contrast core [4].

In Fig. 6, we present the effect of the dielectric contrast on the band gap width. The calculations are performed for each structure at the corresponding densities of maximum band gap width as given in Fig. 5. We clearly see that these photonic crystals possess a photonic band gap if dielectric contrast between the two dielectric material is greater than four.

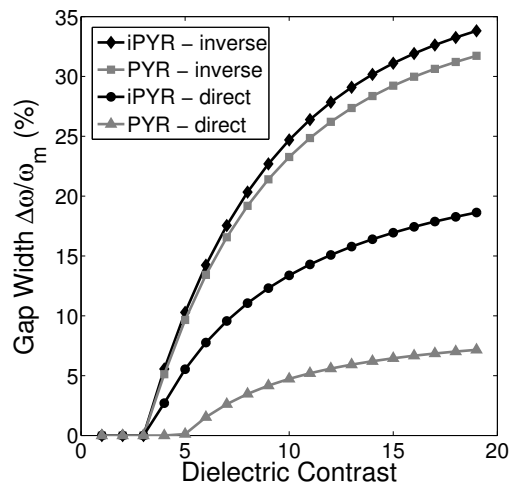


FIG. 6. Effect of dielectric contrast between the high- and low- dielectric constant materials in the photonic crystals calculated for direct and inverse structures of the ideal pyrochlore lattice (iPYR) and the pyrochlore-like structure (PYR) obtained in our simulations. The calculations are performed at (reduced) density given in Fig. 5.

* h.pattabhiraman@uu.nl

† m.dijkstra@uu.nl

- [1] X. Zeng, F. Liu, A. G. Fowler, G. Ungar, L. Cseh, G. H. Mehl, and J. E. Macdonald, *Adv. Mater.* **21**, 1746 (2009).
- [2] M. M. Wojcik, M. Gora, J. Mieczkowski, J. Romiszewski, E. Gorecka, and D. Pocięcha, *Soft Matter* **7**, 10561 (2011).
- [3] B. A. Lindquist, S. Dutta, R. B. Jadrich, D. J. Milliron, and T. M. Truskett, *Soft Matter* **13**, 1335 (2017).
- [4] K. P. Velikov, A. Moroz, and A. van Blaaderen, *Applied Physics Letters* **80**, 49 (2002).